

Observation of modulational instability in Bose-Einstein condensates

P.J. Everitt¹, M.A. Sooriyabandara¹, M. Guasoni², P.B. Wigley¹, C.H. Wei^{1,3}, G.D. McDonald¹, K.S. Hardman¹, P.Manju¹, J.D. Close¹, C.C.N. Kuhn¹, Y.S. Kivshar², and N.P. Robins¹

¹*Department of Quantum Science, Research School of Physics and Engineering,
Australian National University, Canberra ACT 2601, Australia*

²*Nonlinear Physics Center, Research School of Physics and Engineering,
Australian National University, Canberra ACT 2601, Australia*

³*Department of Instrument Science and Technology,
College of Mechatronic Engineering and Automation,
National University of Defense Technology, Changsha 410073, China*

We observe the breakup dynamics of an elongated cloud of condensed Rb⁸⁵ atoms placed in an optical waveguide. The number of localized wave packets observed in the breakup is compared with the number of solitons predicted by a plane-wave stability analysis of the nonpolynomial nonlinear Schrödinger equation, an effective 1D approximation of the Gross-Pitaevskii equation for cigar-shaped condensates. It is shown that the numbers predicted from the fastest growing sidebands are consistent with the experimental data, suggesting that modulational instability is the key underlying physical mechanism driving the breakup.

INTRODUCTION

Intensity-dependent instabilities are a dramatic manifestation of strong nonlinear effects that can occur in nature, and they are observed in many branches of physics as the development of spatial or temporal modulations with growing amplitudes. *Modulational instability* (MI) is a well-known phenomenon in optics which manifests itself as a decay of long optical signals into pulse trains [1–3]. MI is a general wave phenomenon that occurs when a weak perturbation to a waveform is enhanced by nonlinearity giving rise to sidebands in the spectrum with the subsequent modulation growth and the formation of a train of spatially or temporally separated solitary waves [4].

Solitary matter-waves of a different origin have been extensively studied in Bose-Einstein condensates (BECs), where interatomic interactions give rise to strong nonlinearities. In particular, soliton trains in BECs have previously been observed to occur in ⁷Li condensates with attractive interactions loaded into a highly anisotropic trap [5]. The formation of multiple solitary waves has also been observed during collapse of Rb condensate clouds [6]. More recently, BEC solitons have been employed for the first realization of a solitonic atom interferometer [7]. In spite of many theoretical predictions [8–10], the stochastic nature of many of these nonlinear processes, combined with traditionally destructive methods of BEC imaging, has impeded the direct observation of more subtle nonlinear effects.

In this Letter, we present the first real-time observation of modulational instabilities in BECs. Using a non-destructive in-situ imaging technique, we are able to image a single BEC as it undergoes the transformation into a train of localized pulses placed in an optical waveguide. It is shown that the number of localized wave packets observed after the breakup is consistent with an

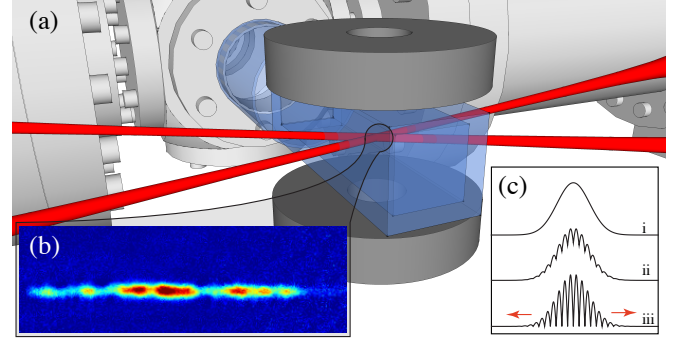


FIG. 1. (a) Schematic of UHV apparatus and an optical waveguide. (b) Soliton train observed after 100 ms propagation of a BEC in the waveguide at $a_s = -1.15a_0$. (c) Modulational instability in a one-dimensional model: (i) an initially localized state becomes (ii) modulated by unstable momentum sidebands which (iii) grow exponentially to produce a train of solitons.

MI analysis conducted in the framework of the nonpolynomial Schrödinger equation [11], suggesting that MI is the underlying physical mechanism driving the observed breakup.

RESULTS

Experimental Approach

The experiment is conducted as follows: a ⁸⁵Rb condensate is formed at an s-wave scattering length of $a_s \approx 300a_0$ in a harmonic trap ($\omega_z = 2\pi \times 7$ Hz axially, $\omega_r = 2\pi \times 70$ Hz radially) before the axial trapping is tuned off creating an optical waveguide for the atoms. The waveguide has a repulsive harmonic potential with frequency $\omega_z = 2\pi \times 3i$ Hz due to curvature in the magnetic potential [7]. Simultaneously, the scattering length

is rapidly jumped to another value ($a_s = [-2.1, 5]a_0$) before the condensate is allowed to evolve in the waveguide for approximately 100ms. In all figures t is the time after this jump has been made, once the condensate is freely propagating in the waveguide. For these initial experimental conditions the chemical potential is $\mu = 6.2\hbar\omega_z$, this is the strongly cigar shaped regime [15]. The longitudinal shape of the condensate has a width (L_z) on the order of tens of micrometers. The choice of initial scattering length is made such that the dimensions of the axially trapped cloud prior to the jump in a_s are similar to those of an axially untrapped soliton at the new (necessarily negative) scattering length. This is determined by a variational method [16]. The condensates are then propagated in the waveguide for a range of scattering lengths, ($a_s/a_0 \in [-6, 6]$).

For propagation at certain negative scattering lengths it is observed that the condensate breaks up into a train of similarly sized, spatially localized clouds. These are observed to be soliton-like in that they are stable under further propagation beyond 90ms. A single run at $-1.15a_0$, typical of the train formation observed, is shown in figure 2. The condensate is stable up until 60ms when train formation is observed to occur. Moreover, for $a_s > -1.15a_0$, three-body-recombination losses are almost negligible ($< 5\%$) in the first-stage dynamics where train formation occurs.

10 runs were conducted for each choice of a_s . The number of spatial components was quantified using an image processing algorithm (demonstrated in supplementary material). Briefly, the images are de-noised then binarised with the number of resulting solitons given by counting the morphological components. Train formation is observed to be stochastic in nature – the same experimental conditions resulting in varying number of constituent clouds. Additional runs were conducted at

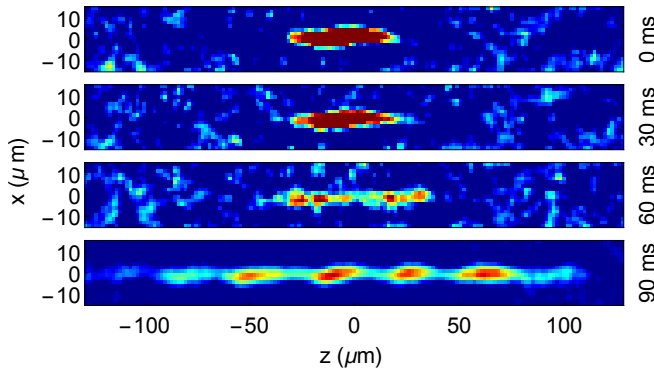


FIG. 2. Experimental data illustrating the breakup phenomenon after BEC is released into the waveguide for a single run with $a_s = -1.15a_0$. The first three images are taken with in-situ non-destructive shadowgraph imaging. The final image is taken by using in-situ destructive absorption imaging with the same optics.

$a_s = -0.75a_0$ and the measured distribution of spatial components shown in Figure 4. Although the atom number varies shot-to-shot by up to 10%, this variation is not correlated with the final number of formed clouds. Variance in the spatial locations of the individual components, in addition to variations in formation onset time were observed.

Theoretical Approach

The nonpolynomial Schrödinger equation (NPSE) [11]—an effective 1D model of the Gross-Pitaevskii equation (GPE)—was used to provide a simple and effective theoretical insight into our experimental observations. It is known to well approximate the full three-dimensional dynamics of the GPE for cigar-shaped condensates whose relevant dynamics takes place in the axial direction [8, 11]. According to the NPSE model, the 3D macroscopic wave-function $\psi(x, y, z, t)$ of the condensate is factorized as the product of unit normalized functions in the axial (z) and transverse (x, y) coordinates, f and ϕ respectively—that is $\psi(x, y, z, t) = f(z, t)\phi(x, y, t; f(z, t))$.

The axial component $f(z, t)$ is the unique unknown of the model, and its spatiotemporal evolution is described by the following equation:

$$i\frac{\partial f}{\partial t} = \left(-c_1 \frac{1}{2} \frac{\partial^2}{\partial z^2} + \frac{c_2}{\sigma^2} |f|^2 + c_3 \left(\sigma^2 + \frac{1}{\sigma^2} \right) \right) f, \quad (1)$$

where $c_1 = \hbar/(2m)$, $c_2 = gN/(2\pi a_\perp^2 \hbar)$, $c_3 = \omega_\perp/2$ and $\sigma^2 = (1 + c_4 |f|^2)^{1/2}$, with $c_4 = 2a_s N$, being: $g = 4\pi\hbar^2 a_s/m$; a_s the s-wave scattering length; N the number of bosons in the condensate; $a_\perp = \hbar^{1/2}(m\omega_\perp)^{-1/2}$ the oscillator length in the transverse direction and ω_\perp the corresponding trapping frequency.

Following the standard procedure [17], in order to describe the MI dynamics in the axial coordinate, the ansatz for $f(z, t)$ is expressed as the sum of a plane wave u and two small perturbations p_1 and p_2 centered at the spatial frequencies $+k$ and $-k$, respectively: $f(z, t) = u \exp(i\beta_u t) + p_1 \exp(ikz + i\beta_1 t + gt) + p_2 \exp(-ikz + i\beta_2 t + gt)$; where u, p_1, p_2 are complex coefficients; $\beta_u, \beta_1, \beta_2$ and g are k -dependent real coefficients; and g represents the temporal growth-rate of the perturbations.

Inserting the ansatz into Eq.(1) and applying a linear stability analysis yields an expression for both $\beta_{u,1,2}$ and g . The latter of these is the gain spectrum of spatial modes with wavenumber k , which is given by:

$$g(k) = \frac{c_1^{1/2} |k|}{2} (4M - c_1 k^2)^{1/2} \\ M = \frac{-(c_2 + c_3 c_4/2) |u|^2}{\sigma_0^2} + \frac{c_2 c_4 |u|^4 + c_3 c_4 |u|^2}{2\sigma_0^6} \quad (2)$$

where $\sigma_0^2 = (1 + c_4 |u|^2)^{1/2}$.

From Eq.(2) it can be shown that all spatial frequencies in the MI-band $-2(M/c_1)^{1/2} \leq k \leq 2(M/c_1)^{1/2}$ undergo amplification and that the fastest growing sidebands are at $\hat{k} = (2M/c_1)^{1/2}$ with a corresponding growth-rate of $\hat{g} = M$.

It is worth noting that in the weakly interacting limit $c_4|f|^2 \ll 1$ Eq.(1) reduces to the well-known 1D-GPE [11], which is less accurate than the aforementioned NPSE model as it fails to describe the condensate dynamics in a non-weakly interacting regime [11]. Therefore Eq.(2) allows accurate descriptions of the growth-rate of perturbations in both weak and strongly interacting regimes.

In the more general and realistic case in which the initial axial function $u_0 = u(z, t = 0)$ is not a plane-wave but finite-sized, it undergoes both a linear reshaping (first term in right-hand-side of Eq.(1)) and a nonlinear reshaping (second and third terms in right-hand-side of Eq.(1)), which are respectively analogous to the diffraction and the nonlinear self-phase modulation (SPM) experienced by an optical beam propagating in a nonlinear Kerr-media [18].

Linear (diffraction) and nonlinear (SPM and MI) effects interplay each other and are characterized by a characteristic time that defines the temporal scale over which they become relevant to the condensate dynamics (more details are reported in the Supplementary Material). Exploiting the analogy with optical phenomena in Kerr-media, the characteristic time for linear diffraction and nonlinear phenomena can be roughly estimated as $T_D = L_z/c_1^2$ and $T_{NL} = 1/(|c_2|u_{pk}^2)$, respectively, where L_z is the spatial width of u_0 whereas $u_{pk} = \max\{|u_0|\}$ is the peak value of its magnitude. According to system parameters, in our experiment $T_D \gg T_{NL}$. Consequently the first stage evolution of the condensate is essentially dominated by MI and can be written as follows:

$$f(z, t) = u_0 e^{i\beta_u t} + \int p_k e^{ikz + i\beta_k t + g_k t} dk \quad (3)$$

where the integration is performed over the whole MI-band and $p_k = p(k)$ indicates the initial perturbation at spatial frequency k that is amplified with growth-rate $g_k = g(k)$ as given by Eq.(2). The perturbation integral in Eq.(3) represents a superposition of sinusoidal waves giving rise to the typical humps observed in the condensate axial profile. If the condensate is seeded by random system noise then the initial perturbation p_k is a stochastic variable whose value depends on the particular experimental run. Consequently, for a fixed time t , the position, amplitude and shape of the humps will be different at each run. This explains the random nature of the humps observed in the experiments and represents a truly distinctive signature of the MI regime.

Figure 3 displays the evolution of a simulated BEC undergoing MI, which resembles the typical evolution ob-

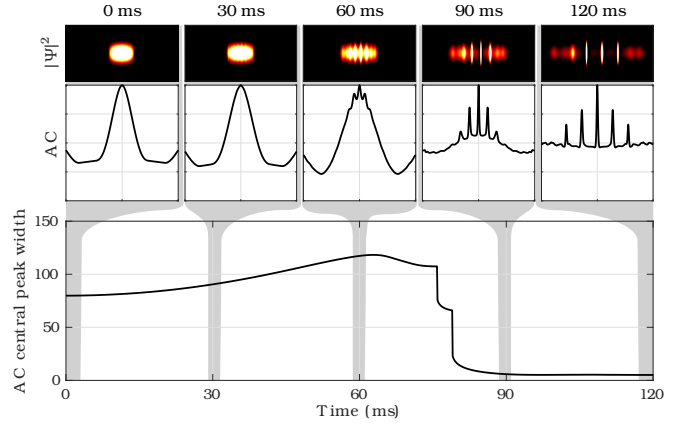


FIG. 3. *Top row:* Density distribution of a simulated BEC undergoing MI in an antitrapping waveguide. Asymmetry in the final distribution is from random noise used to seed the instability. *Middle row:* Autocorrelation (AC) traces of the axial density. *Bottom figure:* Width of the central peak of the autocorrelation of the axial density as a function of time. The sharp change in the central peak width at 75 ms corresponds to the point where the MI is well developed.

served in experiments. The simulations were seeded with Gaussian noise with a minimum spatial correlation width determined by the healing length of the condensate. This ensures that the perturbation doesn't contain nonphysical noise. The amplitude of the noise was approximately 1% of the amplitude of ψ . Condensate breakup gives rise to the formation of spatial components, which become clear and separated once MI amplification is well-developed. The condensate final distribution is typically asymmetric as a result of the random seeding noise used in the simulation.

As each experimental run is independent, seeding noise in each realization is independent as well, therefore the statistical average of the distance d_z between consecutive humps is $\langle d_z \rangle = 2\pi/\hat{k}$, from which the statistical average of the number of humps can be estimated as $\langle N_H \rangle = L_z/d_z$, where the brackets $\langle \rangle$ denote statistical averaging.

We highlight that SPM induces an axial compression of the condensate, which is related to a broadening of the condensate initial axial spectrum, that is the Fourier transform of u_0 . The larger the width Δk of the initial axial spectrum, the faster the spectral broadening and the corresponding spatial compression. When Δk is comparable with or larger than \hat{k} , then the spectral broadening undergone by the axial spectrum overlaps the MI-band so that the amplification of the seeding noise becomes negligible in the condensate dynamics. In this case the SPM-induced spatial compression is followed by complex dynamics that may lead to the creation of distinct spatial components (see Supplementary Material). These dynamics are similar to those undergone by short optical pulses in Kerr-media [18]. However in this circumstance the number, position and shape of the spatial

components are fully deterministic, as they do not depend on the seeding noise.

An intermediate regime exists where neither MI nor SPM are truly dominant, but are equally important to the condensate dynamics. In this instance, the condensate undergoes a partial reshaping followed by the creation of random humps related to the MI (see Supplementary Material). For typical experimental parameters $L_z \sim 50\mu\text{m}$ and $a_s \sim -a_0$ we estimate $\Delta k \sim 1/L_z \approx 20\text{m}^{-1}$ and $\hat{k} \approx 100\Delta k$, therefore SPM does not dominate over MI. However, for sufficiently negative scattering lengths, simulations show that a fast and strong spectral broadening due to SPM occurs, which bring our experiments in the aforementioned intermediate regime.

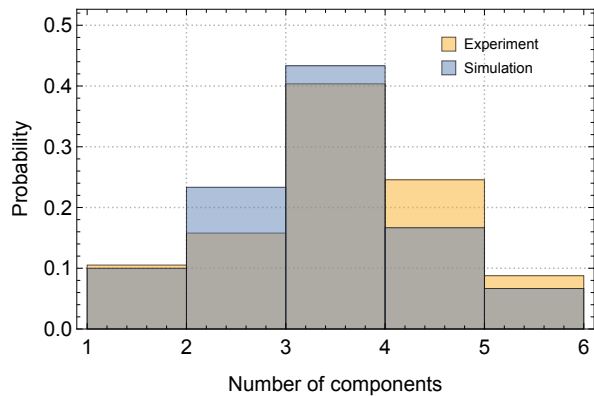


FIG. 4. Probability of observing a given number of spatial components for both experiment and simulations at a scattering length of $-0.75a_0$. Grey regions indicate overlap of both distributions. A total of 57 experimental runs were conducted. The mean number of spatial components for both experiment (3.05 ± 0.14) and simulations (2.87 ± 0.19) agree within the error (calculated as the standard error in the mean)

The stochastic nature of MI which depends on the initial seeding of noise results in a variation of the measured number of components. NPSE simulations reproducing the conditions of the experiment, including the antitrapping potential and three-body recombination losses show the onset of MI for low attractive scattering lengths (the recombination losses appear as an additional term $iK_3 N^2 |f|^4 f / (2\pi a_\perp^2 \sigma^2)^2$ in the RHS of Eq. (1), where $K_3 = 4 \times 10^{-41} \text{m}^6 \text{s}^{-1}$ is an experimentally determined quantity). Good agreement between the statistical distributions of measured number of spatial components for both experiment and simulation is seen in Figure 4. Both the mean (3.05 ± 0.14 for experiment and 2.87 ± 0.19 for simulations) and standard deviation (1.09 ± 0.11 for experiment and 1.04 ± 0.14 for simulations) agree within their standard errors.

A plot of the number of spatial components observed in experiments as a function of a_s is shown in Figure 5 alongside the predictions from a stability analysis of the NPSE as well as NPSE simulations. The difference

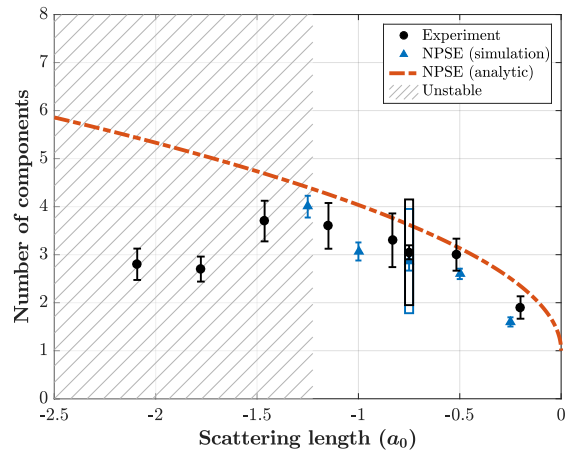


FIG. 5. Number of spatial components observed in experiment at $t=90\text{ms}$ compared with dissipative NPSE simulations and analytic estimation $\langle N_H \rangle = L_z/d_z$ ($\langle d_z \rangle = 2\pi/\hat{k}$). The initial BEC is considered to have one component. Error bars are calculated from the standard error in the mean across multiple runs. Boxes on data points indicate the standard deviation. The single hatched region indicates the absence of a stable soliton solution.

between simulations and analytic estimation is expected due to the presence of a partial SPM pulse reshaping as well as the antitrapping potential not accounted for by our analytical model. Note also that stable soliton solutions of the initial condensate do not exist below $a_s = -1.2$, as determined by a variational analysis of the GPE energy functional [16]. In this unstable region thermal populations in the experiment are measured and mean-field formalism is no longer applicable as it does not capture coupling of the condensate dynamics to the thermal cloud.

DISCUSSION

The observed random position, number and amplitude of measured components is truly indicative of MI dynamics. When taking additional experimental samples for a particular scattering length, agreement with NPSE simulations of MI is seen in both the mean and standard deviation of the number of measured components. On the contrary, if train formation was seeded by linear effects its dynamics are then deterministic, similarly to what occurs with SPM-reshaping. We also point out that although the mean-field formalism employed here cannot account for fragmentation effects captured by the many-body model, the fragmentation dynamics predicted to be observed in an initially symmetric condensate are highly symmetric [10, 19]. Therefore we believe the stochastic breakup dynamics observed in our experiments are a

truly distinctive signature of MI, whereas the observation of symmetric and deterministic behaviour would be suggestive of a different underlying mechanism, such as MI seeded by linear effects from fragmentation or SPM reshaping.

In summary, we have presented the first continuous experimental observation of modulational instability in a single Bose-Einstein condensate. A major advance of our experiments is the ability to image non-destructively stochastic time-dependent nonlinear phenomena with high temporal resolution. Our experimental observations have been found to be in a good agreement with the analytical and numerical predictions provided by the nonpolynomial Schrödinger equation that takes into account a tight confinement of the trap, and they suggest that modulational instability seeded by noise is a key physical mechanism underlying the breakup of elongated condensates into matter-wave solitary waves.

The improvements made to the experimental apparatus will allow the detailed study of many new aspects of nonlinear dynamics driven by modulational instability. For MI to occur, an initial perturbation is required that then exponentially grows. Applying a reproducible initial noise profile to seed the condensate (necessarily greater in amplitude than those already present in the system) would remove the stochastic nature of the MI allowing the timescales and transient dynamics of MI to be closely compared with simulation. Additionally, the solitons here are created by matching the dimensions of the trapped and untrapped clouds when switching off the confining potential and adjusting the scattering length. If instead, a small mismatch in the radial widths of these two solutions is created then a transverse excitation will be present during MI, altering the dynamics in a way not captured by the NPSE. Finally, the role of relative-phase in soliton-soliton interactions, either attractive and repulsive, has previously only been inferred through comparison with GPE simulation [20]. Combining the agile imaging system of the apparatus and the ability to perform Bragg interferometry along the waveguide [7] would allow a direct measurement of this effect. By first non-destructively observing train formation and subsequent soliton interactions, neighboring solitons can then be interfered and their relative phase read out with higher SNR destructive imaging.

Similar work, developed independently, was released just after the preparation of this manuscript which focuses on modulational instability in a Li condensate [21].

METHODS

The experimental apparatus is described in depth in one of the previous works [12]. In summary, a combined two and three-dimensional MOT system collects and cools both ^{85}Rb and ^{87}Rb atoms (see figure 1). The

atoms are then loaded into a magnetic trap and undergo RF evaporation before being loaded into an optical cross trap. The cross trap consists of intersecting 1090 nm and 1064 nm laser beams with approximate waists of $300\mu\text{m}$ and $250\mu\text{m}$ (half-width at $1/e^2$ intensity), respectively. After loading, the magnetic trap coils are switched from anti-Helmholtz to Helmholtz configuration. This allows the s -wave scattering length of the cloud, a_s , to be tuned utilizing a Feshbach resonance. Setting the ^{85}Rb scattering length close to zero ($a_s = 3a_0$) while ramping down the cross trap intensity allows sympathetic cooling to remove the remaining ^{87}Rb atoms while minimizing three-body recombination losses in ^{85}Rb . A further period of evaporation with $a_s = 300a_0$ creates a ^{85}Rb BEC of atom number $N = 3 \times 10^4$ with no observable thermal fraction. This is the initial condition for all experiments discussed below.

To monitor the cloud dynamics two orthogonal imaging systems are available. Firstly, a horizontal absorption beam allows the cloud to be imaged after 20ms of ballistic expansion ($a_s = 0$) in free space to calibrate absolute atom number. A second vertical, far detuned imaging beam utilizes a non-destructive shadowgraph imaging technique to take in-situ images of the condensate [13]. Up to 100 images can be taken in a single run as little as 0.4ms apart with no measurable change in atom number. The imaging laser is offset beat locked, allowing the detuning of the beam to be dynamically changed during a run [14]. This allows several non-destructive pictures to be taken before the laser is brought onto resonance and a final destructive, high signal to noise (SNR) picture is taken with the same optics.

ACKNOWLEDGEMENTS

The work has been supported by the Australian Research Council and NanoPhi program of the European Union.

-
- [1] V. I. Bespalov and V.I. Talanov, Filamentation structure of light beams in nonlinear liquids, *JETP Lett.* **3**, 307 (1966).
 - [2] A. Hasegawa and W. F. Brinkman, Tunable coherent IR and FIR sources utilizing modulational instability, *IEEE J. Quantum Electron.* **16**, 694 (1980).
 - [3] G. P. Agrawal, Modulational instability induced by cross-phase modulation, *Phys. Rev. Lett.* **59**, 880 (1987).
 - [4] Y.S. Kivshar and G. Agrawal, *Optical Solitons: From Fibers to Photonic Crystals* (Academic Press, Boston, 2003).
 - [5] K. E. Strecker, G. B. Partridge, A. G. Truscott, and R. Hulet, Formation and propagation of matter-wave soliton trains, *Nature* **417**, 150 (2002).

- [6] L. Cornish, S.T. Thompson, and C.E. Weiman, Formation of bright matter-wave solitons during the collapse of attractive Bose-Einstein condensates, *Phys. Rev. Lett.* **96**, 170401 (2006).
- [7] G.D. McDonald, C.C.N. Kuhn, K.S. Hardman, S. Bennetts, P.J. Everitt, P.A. Altin, J.E. Debs, J.D. Close, and N.P. Robins, Bright solitonic matter-wave interferometer, *Phys. Rev. Lett.* **113**, 013002 (2014).
- [8] L. Salasnich, A. Parola, and L. Reatto, Modulational instability and complex dynamics of confined matter-wave solitons, *Phys. Rev. Lett.* **91**, 080405 (2003).
- [9] L.D. Carr and J. Brand, Spontaneous soliton formation and modulational instability in Bose-Einstein condensates, *Phys. Rev. Lett.* **92**, 040401 (2004).
- [10] A.I. Streltsov, O.E. Alon, and L.S. Cederbaum, Formation and dynamics of many-body fragmented states in one-dimensional attractive ultracold gases, *Phys. Rev. Lett.* **100**, 130401 (2008).
- [11] L. Salasnich, A. Parola, and L. Reatto, Effective wave equations for the dynamics of cigar-shaped and disk-shaped Bose condensates, *Phys. Rev. A* **65**, 043614 (2002).
- [12] C.C.N. Kuhn, G.D. McDonald, K.S. Hardman, S. Bennetts, P.J. Everitt, P.A. Altin, J.E. Debs, J.D. Close, and N.P. Robins, A Bose-condensed, simultaneous dual-species Mach-Zehnder atom interferometer, *New J. Phys.* **16**, 073035 (2014).
- [13] P. B. Wigley, P. J. Everitt, K. S. Hardman, M. R. Hush, C. H. Wei, M. A. Sooriyabandara, P. Manju, J. D. Close, N. P. Robins, and C. C. N. Kuhn, Non-destructive shadowgraph imaging of ultra-cold atoms, *Optics Letters* **41**, 4795-4798 (2016).
- [14] C. Wei, S. Yan, A. Jia, Y. Luo, Q. Hu, and Z. Li, Compact phase-lock loop for external cavity diode lasers, *Chinese Opt. Lett.* **14**, 051403 (2016).
- [15] D. S. Petrov, G. V. Shlyapnikov, and J. T. M. Walraven, Regimes of Quantum Degeneracy in Trapped 1D Gases, *Phys. Rev. Lett.* **85**, 3745 (2000).
- [16] L.D. Carr and Y. Castin, Dynamics of a matter-wave bright soliton in an expulsive potential, *Phys. Rev. A* **66**, 063602 (2002).
- [17] A. Hasegawa and W. F. Brinkman, Derivation of spatial growth frequencies in NLSE, *IEEE J. Quantum Electron.* **16**, 694 (1980).
- [18] J.M. Dudley, G. Genty, and S. Coen, Supercontinuum generation in photonic crystal fiber, *Rev. of Mod. Phys.* **78**, 1135 (2006).
- [19] L.S. Cederbaum, A.I. Streltsov and O.E. Alon, Fragmented Metastable States Exist in an Attractive Bose-Einstein Condensate for Atom Numbers Well above the Critical Number of the Gross-Pitaevskii Theory, *Phys. Rev. Lett.* **100**, 040402 (2008).
- [20] J.H.V. Nguyen, P. Dyke, De Luo, B.A. Malomed, and R.G. Hulet, Collision of matter-wave solitons, *Nature Physics* **10**, 918-922 (2014).
- [21] J.H.V. Nguyen, De Luo, and R.G. Hulet, Formation of matter-wave soliton trains by modulational instability, *arXiv:1703.04662* (2017).